

Multifunctional polymers based on ionic liquid and Rose Bengal fragments for the conversion of CO₂ to carbonates.

David Valverde,^[a] Raúl Porcar,^[a,c] Pedro Lozano,^[b] Eduardo García-Verdugo,*^[a] Santiago V. Luis*^[a]

- [a] Dpt. of Inorganic and Organic Chemistry, Supramolecular and Sustainable Chemistry Group
University Jaume I. Avda Sos Baynat s/nE-12071-Castellon
E-mail: cepeda@uji.es luiss@uji.es
- [b] Dep. Bioquímica y Biología Molecular "B" e Inmunología. Universidad de Murcia. Campus de Espinardo, E-30.100. Murcia, Spain
- [c] Departamento de Química Orgánica y Bio-Orgánica, Facultad de Ciencias, UNED, Paseo Senda del Rey, 9, E-28040, Madrid, Spain

Index.

Table S1. Structure and properties for the different SILLPs prepared.	S2
Fig. S1. Swelling of RB-SILLPs resins in styrene oxide.	S3
Fig. S2. FT-IR-ATR for the RB-SILLPs, with expansion of the ν(O-H) region, showing the uptake of water from air for the different low loading gel-type PS-DVB resins with different substitution patterns.	S4
Fig. S3. FT-IR-ATR for the RB-SILLPs, with expansion of the ν(O-H) region, showing the uptake of water from air for the different of low loading macroporous type PS-DVB resins with different substitution patterns.	S5
Fig. S4. FT-IR-ATR for the RB-SILLPs, with expansion of the ν(O-H) region, showing the uptake of water from air for the different RB-SILLPs prepared from gel type PS-DVB resins with different loadings.	S6
Fig. S5. FT-IR-ATR for the RB-SILLP 23b . a) before its use as catalyst. b) After the catalytic use.	S7
Fig. S6. Synthesis of the polymer-supported zwitterionic NHC-CO ₂ species.	S8
Fig. S7. FT-IR-ATR for RB-SILLP 17a a) before and b) after its use as catalyst.	S9
Fig. S8. FT-IR-ATR for RB-SILLP 25b a) before and b) after its use as catalyst.	S10
Fig. S9. FT-IR-ATR for a) Merrifield resin 2 . b) resin 26 . c) resin 27 .	S11
Fig. S10. FT-IR-ATR for SILLP 8a a) before and b) after its use as catalyst.	S12
Table S2. Comparison of RB-SILLP 27 with relevant catalysts reported in the literature for the cycloaddition of CO ₂ to epoxides under continuous flow conditions.	S13

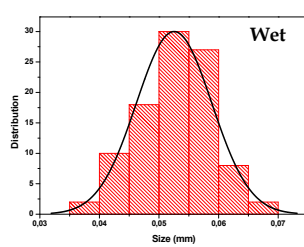
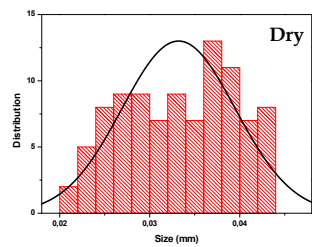
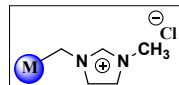
Table S1. Structure and properties for the different SILLPs prepared.

Structure	Code	Type	Loading (meq/g)	R	R'	Water content [a] (%)	Swelling (%) ^[c]
	7a	Gel	1.01	CH ₃	H	1.81	56
	8a	Macroporous	1.09	CH ₃	H	3.46	-
	9a	Gel	0.97	CH ₄ H ₉	H	1.27	69
	10a	Macroporous	1.94	CH ₄ H ₉	H	2.62	-
	11a	Gel	0.88	CH ₁₀ H ₂₁	H	1.27	81
	12a	Macroporous	0.95	CH ₁₀ H ₂₁	H	2.10	-
	13b	Gel	3.18	CH ₃	H	11.35	-
	14b	Macroporous	3.79	CH ₃	H	15.14	-
	15b	Macroporous	3.71	CH ₃	CH ₃	-	-
	16a	Gel	1.01	CH ₃	H	2.01	-
	17a	Macroporous	1.09	CH ₃	H	3.50	-
	18a	Gel	0.97	CH ₄ H ₉	H	-	-
	19a	Macroporous	1.94	CH ₄ H ₉	H	2.60	-
	20a	Gel	0.88	CH ₁₀ H ₂₁	H	1.17	-
	21a	Macroporous	0.95	CH ₁₀ H ₂₁	H	2.10	-
	22b	Gel	3.18	CH ₃	H	-	-
	23b	Macroporous	3.79	CH ₃	H	-	-
	24b	Macroporous	3.71	CH ₃	CH ₃	-	-
	25b	Macroporous	3.68	CH ₃	H	-	-
	26	Macroporous	1.56	CH ₃	H	-	-
	27	Macroporous	2.23	CH ₃	H	-	-
	30a	Gel	1.1	CH ₃	H	-	-
	31b	Macroporous	3.67	CH ₃	H	-	-

[a] Water content calculated from TGA, after equilibration at rt during 24 h. [b] RB loading $3.92 \times 10^{-2} \mu\text{mol RB / g of polymer}$. [c] $\text{Swelling} = \left(\frac{\text{Wet size} - \text{Dry size}}{\text{Dry size}} \right) \cdot 10^2$

a)

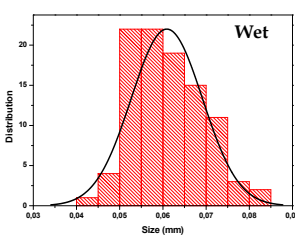
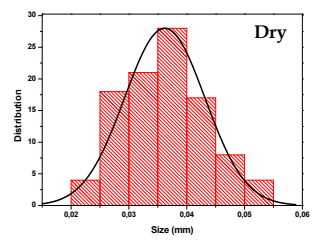
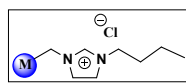
Swelleling 7a
(g) 1.2 meq/g



Swelling: 56%

b)

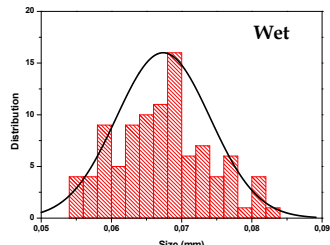
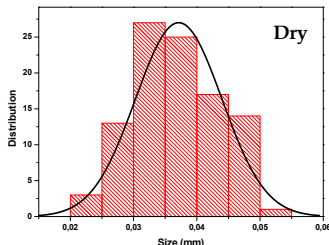
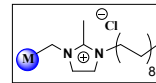
Swelleling 9a
(g) 1.2 meq/g



Swelling: 69%

c)

Swelleling 11a
(g) 1.2 meq/g



Swelling: 81%

Fig. S1. Swelling of different RB-SILLPs resins in styrene oxide (SO) calculated as (a) 7a. (b) 9a. (c) 11a. $\text{Swelling} = \left(\frac{\text{Wet size} - \text{Dry size}}{\text{Dry size}} \right) \cdot 10^2$. For each resin, the size distribution diagram on the left corresponds to the dry state, while the one on the right correspond to the size distribution in the presence of SO.

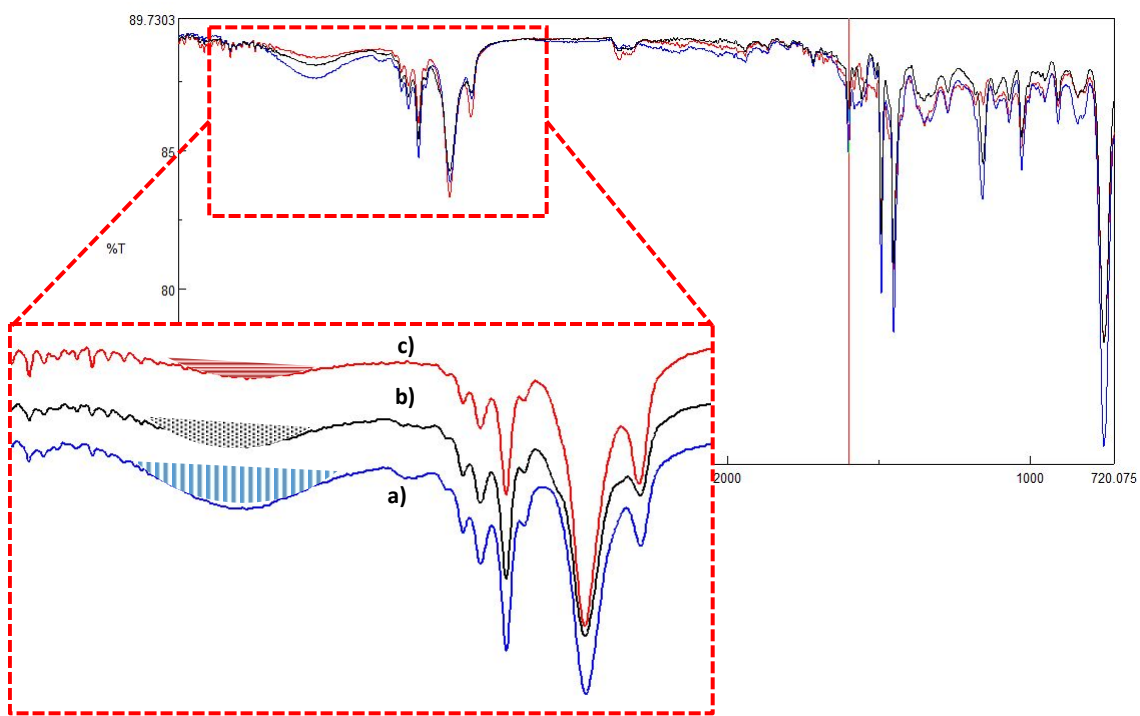


Fig. S2. FT-IR-ATR spectra obtained for the RB-SILLPs of $\nu(\text{O}-\text{H})$ region showing the uptake of water from air as for the different low loading gel-type PS-DVB resin with different substitution pattern. a) **16a** (methyl). b) **18a** (butyl). c) **20a** (2-methyl-decyl).

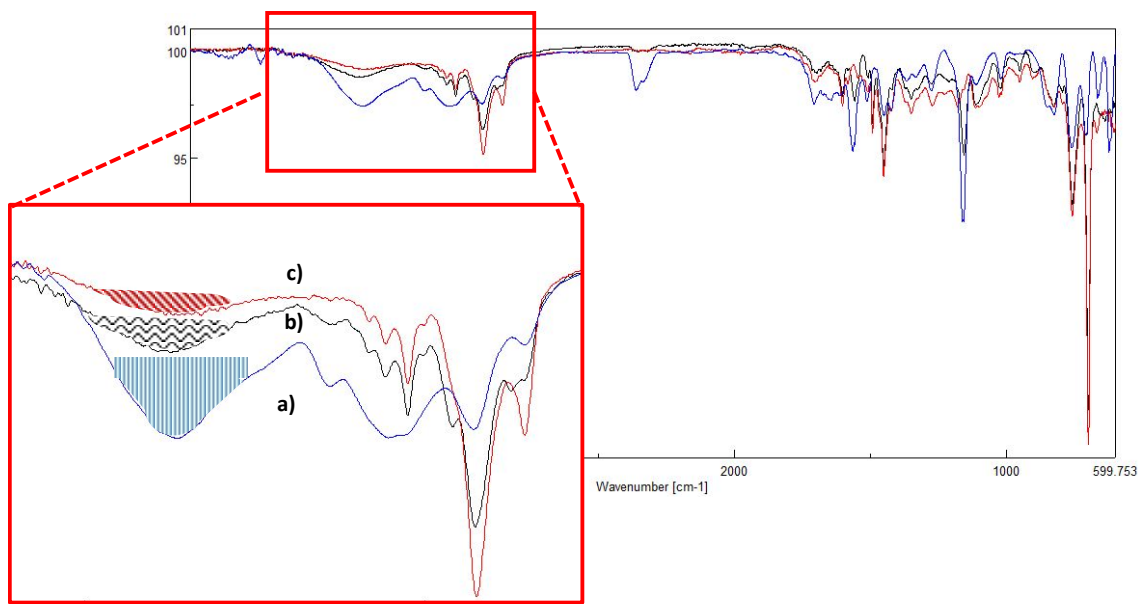


Fig. S3. FT- IR-ATR spectra obtained for the RB-SILLPs of $\nu(\text{O}-\text{H})$ region showing the uptake of water from air as for the different of low loading macroporous type PS-DVB resin with different substitution pattern, a) **17a** (methyl). b) **19a** (butyl). c) **21a** (2-methyl-decyl).

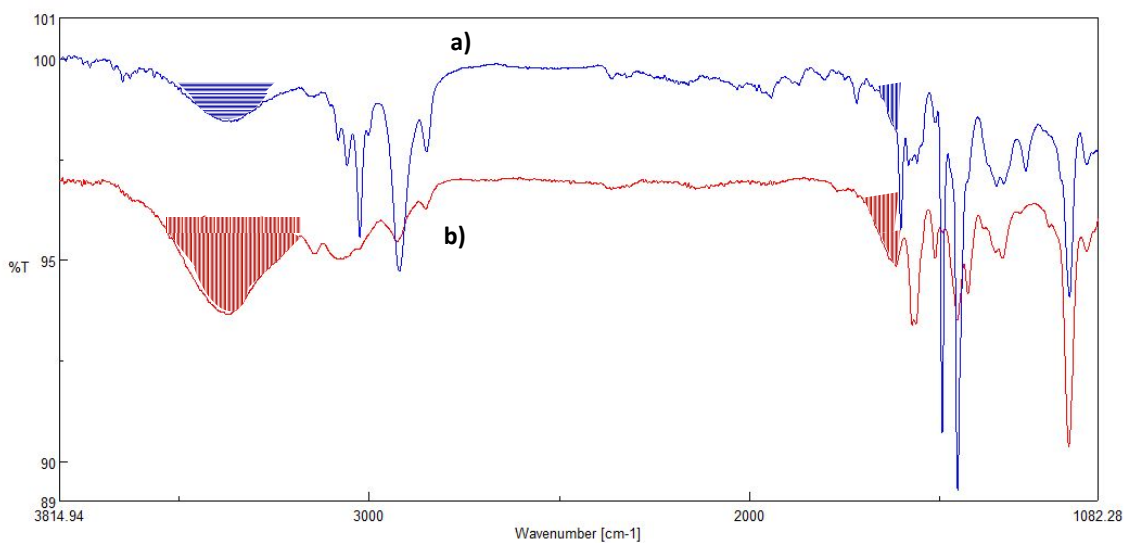


Fig. S4. FT-IR-ATR spectra obtained for the RB-SILLPs of $\nu(\text{O}-\text{H})$ region showing the uptake of water from air as for the different for the RB-SILLPs of gel type PS-DVB resins with different loading. a) Low loading (**16a**). b) High loading (**22b**).

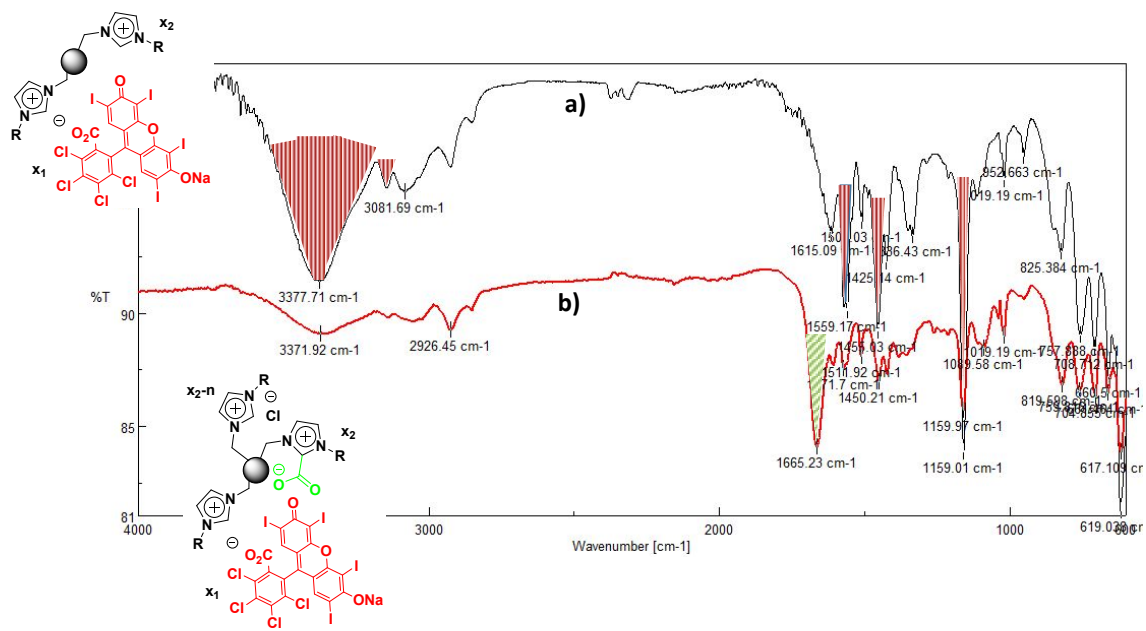


Fig. S5. FT-IR-ATR spectra obtained for the RB-SILLP **23b** a) before its use as catalyst. b) After its use in the catalytic reaction (36.7 mg RB-SILLP **23b**, for 5 h at 100 °C, 10 bar of CO₂ and using 1 mL epoxide).

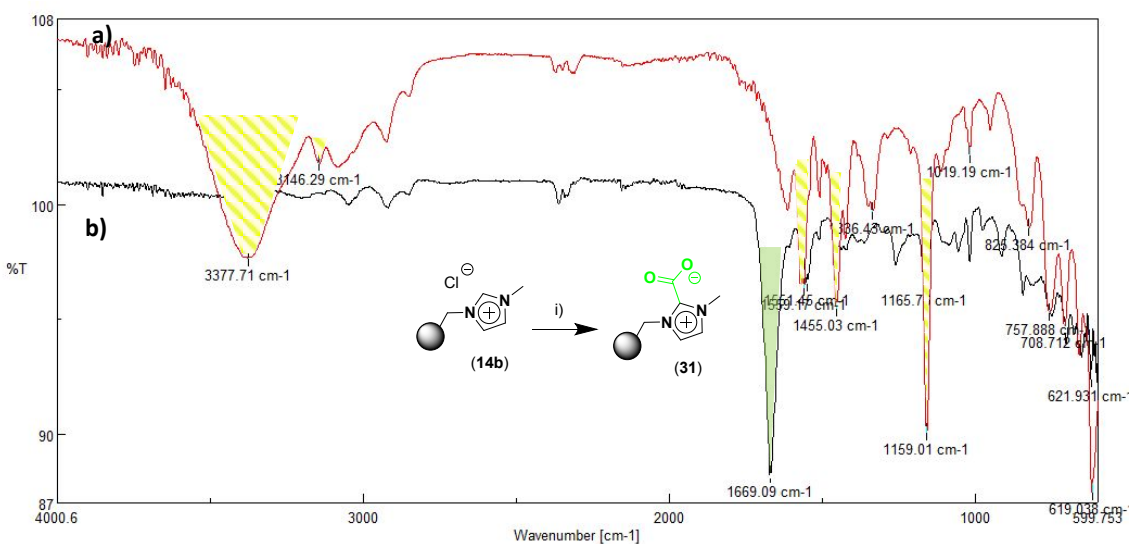


Fig. S6. FT-IR-ATR spectra for the synthesis of the zwitterionic NHC-CO₂ polymer **31** from **14b** (from a high loading chloromethylated resin, macroporous). i) Resin **14b** in 1.0 mL of dry THF, 8.5 equivalents of KHMDS at 80 °C and CO₂ (balloon). a) **14a**. b) **31**.

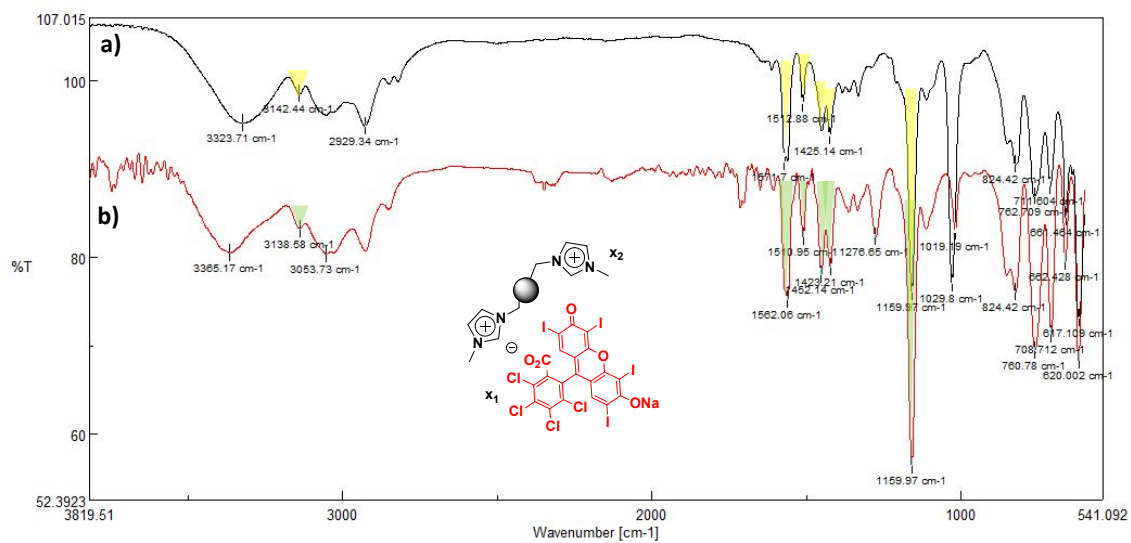


Fig. S7. FT-IR-ATR for RB-SILLP **17a**, a) before and b) after its use as catalyst (reaction conditions: solventless, 5 h, 100 °C, 10 bar CO₂, 1, mL epoxide and 36.7 mg catalyst).

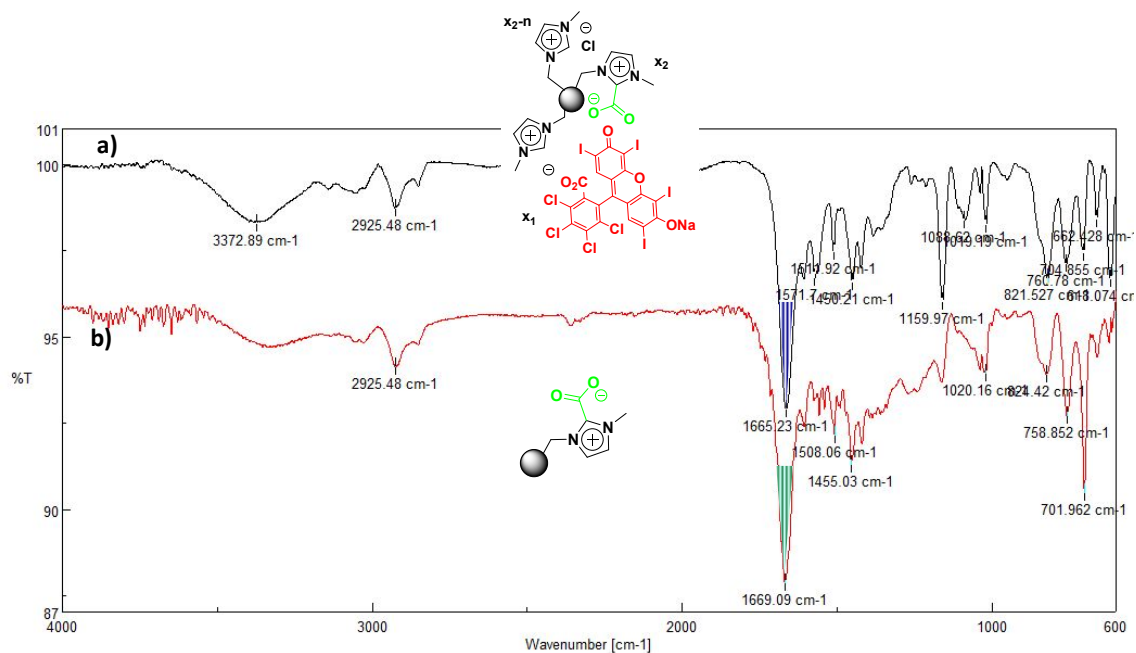


Fig. S8. FT-IR-ATR for RB-SILLP **25b** a) before and b) after its use as catalyst (reaction conditions: 5 h, 100 °C, 10 bar of CO₂ and using 1 mL epoxide and 36.7 mg of catalyst).

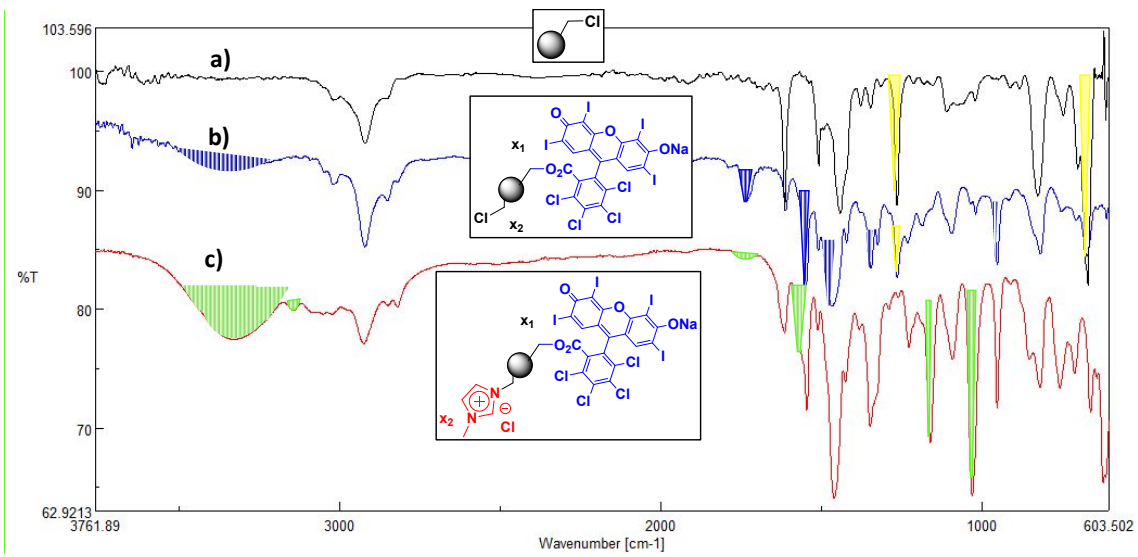


Fig. S9. FT-IR-ATR spectra obtained for a) Merrifield resin **2**. b) resin **26**. c) resin **27**.

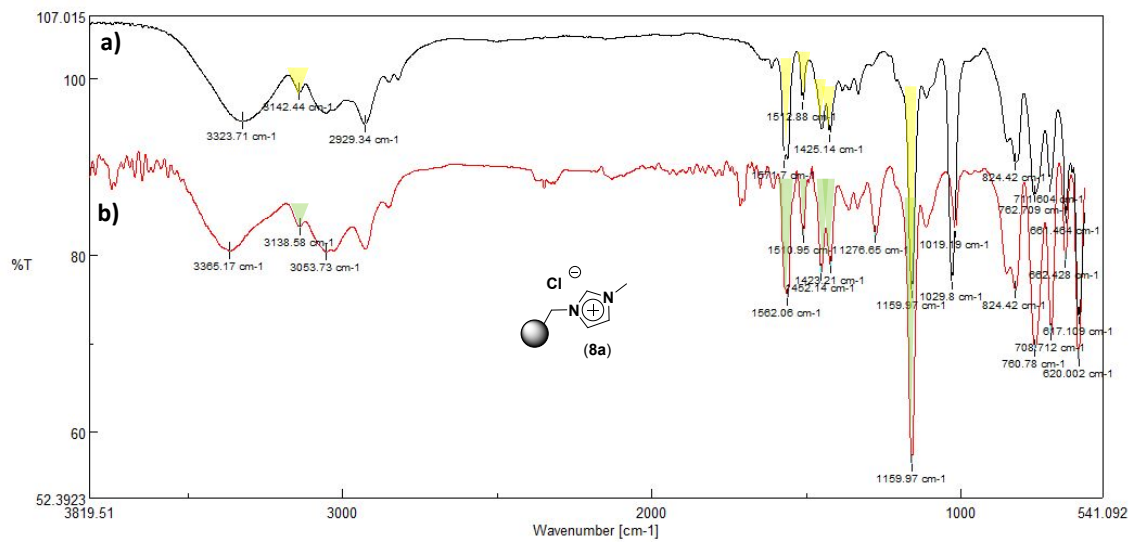


Fig. S10. FT-IR-ATR for SILLP **8a** a) before and b) after its use as catalyst (reaction conditions: 5 h, 100 °C, 10 bar of CO₂ and using 1 mL epoxide and 36.7 mg of catalyst).

Table S2. Comparison of SILPs **27** with relevant catalysts reported in the literature for cycloaddition of CO₂ under flow continuous.

Entry	Catalyst	(g)	Cocatalyst	Solvent	Substrate ^a	Flow Substrate (mL/min)	Flow CO ₂ (mL/min)	Flow N ₂ (mL/min)	Pressure (bar)	Temp. (°C)	Time / Activity (h)	Yield (%)	Prod. _T (g epoxide x g cat ⁻¹ x h ⁻¹)	Prod. _{Exp} (g epoxide x g cat ⁻¹ x h ⁻¹)	Leaching ^b
1	27	1.9	RB/H ₂ O	-	SO	0.005	0.05	-	140	150	234	57	1.9808	1.1291	X
2	MCM-41/[Co(II)(salen)]	4	<i>n</i> -Bu ₄ NBr	-	EO	0.17	0.33	-	125	110	24	86	0.0901	0.775	X
3	Amorphous silica/[salem)Al] ₂ OtBu	0.43	-	-	EO	0.0025	0.017	0.042	1.01	150	6	57	0.3159	0.1801	✓
4	MCM-41/[salem)Al] ₂ OtBu	1.57	-	-	EO	0.0025	0.017	0.042	1.01	60	7	95	0.0865	0.0822	✓
5	Cs-P-Si-oxide	10	-	-	PO	0.05	0.2	-	140	200	3	50	0.0152	0.0076	✓
6	MOF MIL-101(Cr)	0.042	TBABr	Chlorobenzene	PO	0.25	4	-	50	100	5	80	1.0676	0.8541	✓
7	MOF MIL-101(Sc)	0.042	-	-	PO	0.25	4	-	50	100	5	57	1.0676	0.6085	✓

^a: SO: Styrene oxide; EO = Ethylene Oxide; PO = Propylene Oxide.

^b: X = No leaching; ✓ = Leaching

Entry (References):

2. Chemical fixation of CO₂ to ethylene carbonate under supercritical conditions: continuous and selective. X.-B. Lu, J.-H. Xiau, R. He, K. Jin, L.-M. Luo, X.-J- Feng, *Appl. Catal. Gen.* **2004**. 275. 73–78.
- 3 & 4. A Gas-phase flow reactor for ethylene carbonate synthesis from waste carbon dioxide. M. North, P. Villuendas, C. Young, *Chem. Eur. J.* **2009**. 15. 11454-11457.
5. T. Non-halogen catalysts for propylene carbonate synthesis from CO₂ under supercritical conditions. H. Yasuda, L.-H. He, T. Takahashi, T. Sakakura, *Appl. Catal. Gen.* **2006**. 298. 177-180.
- 6 & 7. Structure activity relationships in metal-organic framework catalysts for the continuous flow synthesis of propylene oxide carbonate from CO₂ and propylene oxide. B. R. James, J. A. Boissonnault, A. G. Wong-Foy, A. J. Matzger, M. S. Sanford, *RSC. Adv.* **2018**. 8. 2132-2137

